RESEARCH PAPER

Ball Milling and Post Annealing as an Effective Route to Synthesize $Co_{1-x}Cu_xSbS$ Paracostibite Thermoelectric Material

A. Ostovari Moghaddam[1,2,4,*], A. Shokuhfar[1] and A. Cabot[2,3]

** Ostovary@aut.ac.ir*

Received: June 2018 **Revised:** March 2019 **Accepted:** June 2019

[1] Advanced Materials and Nanotechnology Research Laboratory, Faculty of Materials Science and Engineering, K. N. Toosi University of Technology, Tehran, Iran.

[2] Catalonia Institute for Energy Research, IREC, 08930 Sant Adrià de Besòs, Spain.

[3] ICREA, Pg. Lluis Companys 23, Barcelona, Spain.

[4] South Ural State University (National Research university), 76, Lenin Prospekt, Chelyabinsk, Russia.

DOI: 10.22068/ijmse.16.4.20

Abstract: *Metal sulfides containing non-toxic and earth-abundant elements have emerged as new environmentally friendly thermoelectric materials. In the present work, a new, fast and large scale route to synthesize bulk nanostructured $Co_{1-x}Cu_xSbS$ paracostibite is presented. Stoichiometric compositions of $Co_{1-x}Cu_xSbS$ nanoparticles with $0 \leq x \leq 0.08$ were first processed by high energy ball milling for 3 h and then annealed at different temperatures between 400 ºC to 650 ºC for 1 h. The phase transformations and diffusion process during annealing were thoroughly studied by X-ray diffraction (XRD) and scanning electron microscopy (SEM). Agglomerated nanoparticles with sizes in the range from 40 nm to 80 nm were obtained after 3 h of ball milling and remained below 100 nm after annealing and hot pressing. The thermoelectric properties of hot-pressed samples, including the Seebeck coefficient (S), electrical conductivity (σ) and thermal conductivity (κ), were measured from room temperature up to 723 K. All the samples exhibited a p-type semiconductor character at room temperature and underwent a transition from p-type to n-type conduction above 473 K. Maximum ZT value of 0.12 was obtained for Co0.06Cu0.04SbS4 at 723 K.*

Keywords: *CoSbS, Thermoelectric, Nanostructure, Conduction type, Cu-doping.*

1. INTRODUCTION

Thermoelectric (TE) materials have fascinated us for more than one century as they can directly convert wasted heat into useful electricity. The energy conversion efficiency of a TE material can be estimated from a dimensionless figure of merit $ZT = (S^2\sigma/\kappa)T$, where σ, S, κ and T are electrical conductivity, Seebeck coefficient, thermal conductivity, and temperature, respectively [1,2]. Maximizing the power factor ($S^2\sigma$) and reducing thermal conductivity are the two approaches used to increase ZT values. However, as σ, S and κ are interconnected and it is an arduous challenge to improve one of the parameters without worsening another. Therefore, increase in TE power output has been accompanied by limited success [3-5].

Besides high efficiency, the development of TE materials consisting of non-toxic and earth-abundant elements is also crucial for large scale practical applications. The current state of the art TE materials, such as BiTe, [6,7] and PbTe [8], contains Te, which is toxic and a rare element in the earth's crust. Thus, new TE materials consisting of non-toxic and earth-abundant elements are needed and are very actively searched [9-11]. In this regard, some metal sulfides have emerged as promising TE compounds after discovering high ZT value in tetrahedrite ($Cu_{12}Sb_4S_{13}$) compounds [12-14]. In recent years, numerous attempts have been made to improve ZT values of tetrahedrite through doping with suitable elements [15-17]. Bornite (Cu_5FeS_4), another p-type sulfide-based TE material, was also developed during recent years [18-20]. High ZT values of 0.5 [21], 0.6 [22] and 0.8 [23] have been obtained for these materials through doping, co-doping and judicious control of composition, respectively. Along with these p-type sulfide compounds, paracostibite (CoSbS) has been proposed as a promising n-type sulfide-

based TE material [24,25]. CoSbS crystallizes in an orthorhombic structure space group Pbca with unit cell parameters of a = 5.842, b = 5.951, c = 11.666 Å [25]. High power factors of 1.6 $mWm^{-1}K^{-2}$ at 723K [26] and 2.7 [24] $mWm^{-1}K^{-2}$ at 543K have been achieved when CoSbS is doped by partially substituting Co with Ni and Sb with Te, respectively. However, the main routes to synthesize CoSbS, high-temperature solid-state reaction [27] or ball milling for 20 h [26], are time-consuming and not suitable for large scale production. Thus, the goal of this study is to investigate the TE properties of CoSbS synthesized by a new route and survey the effect of Cu substitution for Co on its performance.

2. EXPERIMENTAL PROCEDURES

Polycrystalline $Co_{1-x}Cu_xSbS_4$ ($0 \leq x \leq 0.08$) nanopowders were obtained by mechanical alloying of cobalt, antimony, copper and sulfur powders in a high energy SPEX 8000 ball mill under high purity argon atmosphere. All powders were purchased from Sigma-Aldrich with a purity higher than 99.5 %. A 70 mL jar and balls (with diameter between 6-10 mm) made from SPK tool steel were used for the milling. The ball to powder mass ratio was adjusted in 10:1, and a rotational speed of 1000 rpm was used. The net milling time was 3 h and a total 10 g of powder was synthesized in each experiment. During milling, the device was ceased and allowed to cool down for 20 minutes after every 10 minutes of milling. Stearic acid, $CH_3(CH_2)_{16}CO_2H$ (2 wt%) was employed as the process control agent. The powder weighting and jar-filling tasks were carried out inside a glove box under high purity argon atmosphere. The milled powders were then annealed at different temperatures ranging from 400 ºC to 650 ºC for 1 h under Ar atmosphere. The resulting powders were then loaded into graphite dies and consolidated into pellets (Ø10 mm × ~1.5 mm) under Ar atmosphere using a custom-made hot press. The hot press was performed at 450 ºC for 5 min, under a pressure of 100 MPa. The densities of the pressed pellets were higher than 80% of the theoretical value in all samples.

A Bruker AXS D8 ADVANCE X-ray diffractometer using Cu–Kα radiation (λ = 0.154 06 Å) with a dwell time of 0.8 s per step and step size 0.03° was employed for XRD studies. The crystallite size (d) was calculated using the Williamson-Hall (W-H) method according to the following equation:

$$\beta \cos\theta = \frac{k\lambda}{d} + 2\varepsilon \sin\theta \qquad (1)$$

where β is the FWHM, corrected for the instrument broadening, λ the x-ray wavelength (1.5406 Å), κ a constant (0.9), ε the lattice strain, d the crystallite size and θ the diffraction angle [20].

The size and morphology of the samples were studied using Zeiss Libra 120 transmission electron microscopy (TEM), operated at 120 kV, and Zeiss Auriga scanning electron microscope (SEM), at 5.0 kV. The elemental analysis of the samples was performed with energy-dispersive X-ray spectroscopy (EDS).

The electrical resistivity and the Seebeck coefficient were measured simultaneously using LSR-3 LINSEIS apparatus over the temperature range of 300 to 723 K under helium atmosphere. The thermal conductivity was obtained as a product of thermal diffusivity (λ), heat capacity (Cp), and mass density of the specimen (ρ), ($\kappa = \lambda \times \rho \times Cp$). XFA 600 Xenon Flash apparatus was employed to measure thermal diffusivities, the density values were obtained using the Archimedes' method and the Dulong-Petit approximation of specific heat (Cp) was used.

3. RESULTS and DISCUSSION

3.1. Structural Evolution

The x-ray diffraction patterns of the as-milled CoSbS powders at different times are shown in Fig. 1a. The XRD pattern of Sb (PDF#083-1323) is also shown in Fig.1a to follow the evolution of powders during ball milling. After 30 minutes of MA, the XRD pattern corresponded to a mixture of antimony, sulfur, and cobalt. The peaks of Sb were still present after 3 h of MA. Some traces of unreacted cobalt could be also detected even after 3 h of high energy MA. As the milling time increased, the intensities of all available planes

[DOI: 10.22068/ijmse.16.4.20]

decreased, but no significant reactions occurred. However, a trace amount of CoSbS (indicated with @ symbol) had nucleated after 3 h of MA. The final composition of powders after 3 h of milling was consistent with the presence of poorly crystalline Sb, S, and Co along with a trace of CoSbS.

The phase transformation of the as milled powders during subsequent annealing can be assessed in Fig.1b. The diffraction patterns of CoSbS and Sb is also shown in Fig.1b. It can be clearly seen that annealing at 450 ºC and lower temperatures resulted in a mixture of $Co_{24}S_{32}$ (linnaeite), CoSbS (costibite) and CoSbS (paracostibite). The amount of linnaeite and costibite phases significantly decreased in the sample annealed at 500 ºC, while the formation of CoSbS (paracostibite) did not proceed completely at this temperature. The XRD pattern of the sample annealed at 550 ºC was consistent with the presence of nearly pure CoSbS with a trace amount of linnaeite. Finally, the XRD pattern of the sample annealed at 650 ºC implied that a pure CoSbS phase with no evidence of impurities such as linnaeite and costibite has been obtained. These results indicated that high energy MA followed by an annealing treatment at 650 °C is a suitable route to produce pure CoSbS.

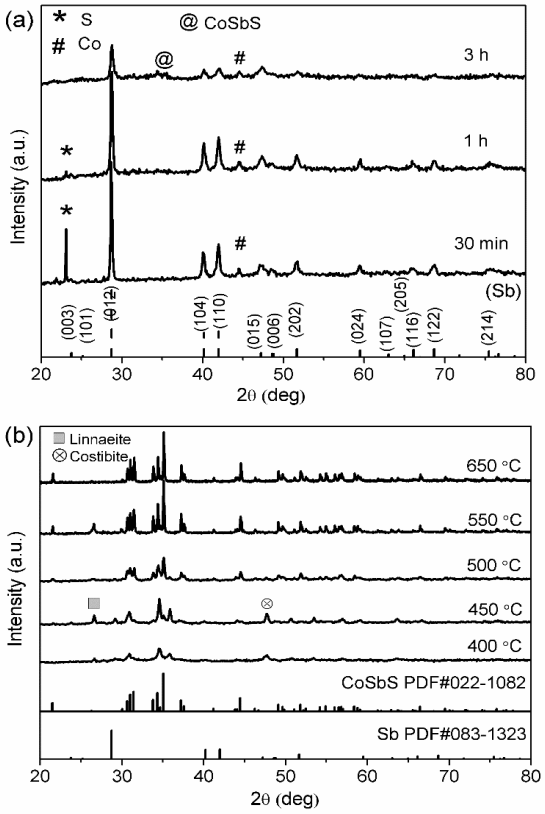

Fig. 1. XRD patterns of as-milled (a) and annealed (b) Co-Sb-S powders. The diffraction patterns of Sb and CoSbS are also shown.

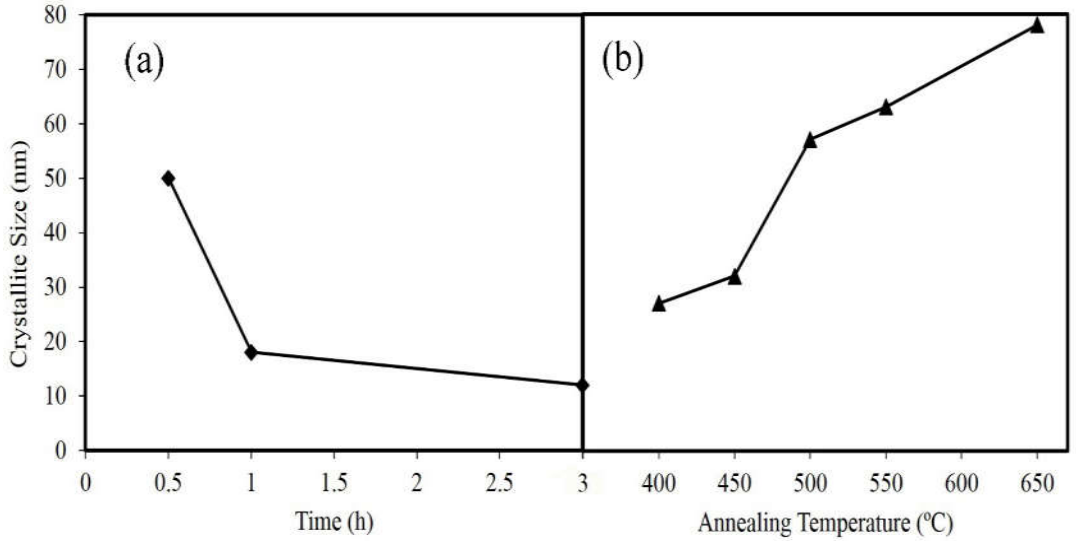

Fig. 2. Crystallite size as a function of milling time (a) and annealing temperature (b).

[DOI: 10.22068/ijmse.16.4.20]

The crystallite size of nanopowders was obtained from the y-axis intersection of the W-H line (βcosθ vs. sinθ). The results are shown in Fig. 2. The crystallite size decreased to 12 nm after 3 h of MA and then increased to 78 nm during annealing at 650 ºC. Severe plastic deformation during MA lead to the creation of thermodynamically unfavorable amount of defects such as vacancies and dislocations, hence a high level of enthalpy is stored in the nanopowder. During annealing, recovery proceeds through dislocations removal or re-arrangement to generate sub-grains, followed by formation of new grains in the recrystallization stage and finally grain growth in the third stage of annealing. Here, it can be clearly seen that the annealing step drove the sample up to the last stage, grain growth, and crystallite size increased from 12 nm for the as milled sample to 78 nm for the annealed sample.

A representative TEM image of the as-milled CoSbS nanoparticles is shown in Fig. 3a. Faceted structures and some rod-like particles with sizes ranging from 40-80 nm can be observed after 3 h of ball milling. A slight inhomogeneity could be also detected in nanoparticles. This shows that the diffusion process required for the formation of the CoSbS phase was not completed even after 3 h of ball milling. So, a posterior annealing process was required to stimulate the long-range diffusion and subsequently formation of CoSbS phase, as seen in the XRD results. An SEM image obtained from the fracture surface of hot-pressed CoSbS sample is also shown in Fig. 3b. The main morphological characteristic of the hot-pressed sample is the presence of coalesced nanoparticles (smaller than 100 nm) with explicit boundaries, while some larger particles can also be detected in Fig. 3b. As microstructural features with a size less than 1 µm are effective in reducing thermal conductivity through hampering the propagation of small wavelength phonons [21], a relatively low thermal conductivity can be expected for all samples. EDS analysis of samples also showed good agreement with the nominal composition of the initial powder mixtures (Table 1).

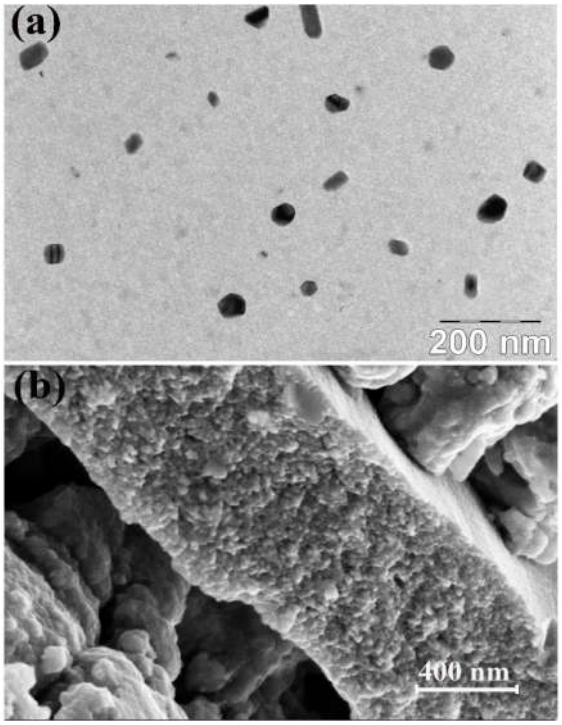

Fig. 3. (a) TEM image of as milled CoSbS nanoparticles and (b) SEM image of the fracture surface of hot-pressed CoSbS.

Table 1. Chemical composition of $Co_{1-x}Cu_xSbS_4$ samples

$Co_{1-x}Cu_xSbS_4$ sample	Nominal composition		EDS Chemical Composition (wt.%)				EDS Formula
			Co	Cu	Sb	S	
$x = 0$	CoSbS	P1	27.658	0	56.923	16.039	$CoSb_{0.97}S_{1.03}$
		P2	28.438	0	55.623	15.469	
		P3	28.018	0	56.127	15.708	
$x = 0.04$	$Co_{0.96}Cu_{0.04}SbS$	P1	27.458	0.962	56.733	16.048	$Co_{0.97}Cu_{0.03}Sb_{0.98}S_{1.02}$
		P2	27.038	0.865	55.802	15.069	
		P3	26.686	0.879	57.027	15.408	
$x = 0.06$	$Co_{0.94}Cu_{0.06}SbS$	P1	27.658	2.091	56.922	16.039	$Co_{0.91}Cu_{0.07}Sb_{0.98}S_{1.04}$
		P2	28.438	1.941	55.623	15.469	
		P3	28.018	2.300	56.127	15.708	

[DOI: 10.22068/ijmse.16.4.20]

3.2. Thermoelectric Properties

The temperature dependence of the electrical resistivity, Seebeck coefficient and the resultant power factor for $Co_{1-x}Cu_xSbS_4$ (x =0, 0.04 0.06) samples are plotted in Fig. 4. It can be seen that the electrical resistivity decreased with increasing temperature (Fig. 4a), which is a typical non-degenerate semiconductor transport behavior. The electrical resistivity of CoSbS was 3.7888 and 0.1046 mΩ·m at room temperature and 723 K, respectively. It should be noted that these resistivity values are close to the values reported by Chmielowski et al. [24] and Yao et al [27]. The electrical resistivity decreased upon substitution of copper for cobalt. Surprisingly, positive Seebeck coefficient values were measured in the low-temperature range, from room temperature and up to about 500 K, pointing toward p-type conduction (Fig. 4b). At temperatures above 500 K, CoSbS showed n-type conduction. It has been reported previously that CoSbS is an n-type material having a Seebeck coefficient in the range of -300 μV/K to -500 μV/K at room temperature [24-27]. However, a distinct behavior from that reported by Chmielowski et al. [24], Yao et al. [27] and Liu et al. [26], who all reported n-type conduction for CoSbS in the entire temperature range, was observed here for CoSbS and Cu-doped CoSbS samples. The highest Seebeck coefficient of -185.74 μV/K at 732 K was obtained for the CoSbS sample. Furthermore, the Seebeck coefficient at first increased and then decreased with increasing temperature. The same trend was observed for all Cu substituted samples. We attribute these different findings to our new synthesized route and, likely, due to the existence of minor impurities such as linnaeite and costibite which cannot be detected in XRD analysis. The maximum power factor of 0.3299 mW/mK^2 was also obtained for un-doped CoSbS. Therefore, a highly reliable procedure was developed here to synthesis CoSbS samples showing a reversible switching between p- and n-type conduction at 500 K.

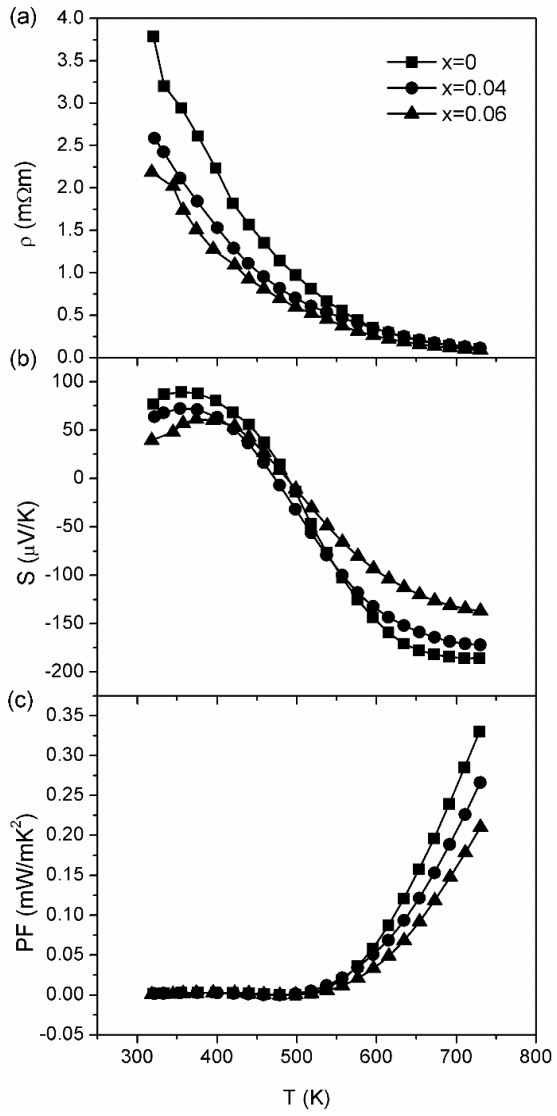

Fig. 4. Transport properties of $Co_{1-x}Cu_xSbS_4$ as a function of temperature; (a) electrical resistivity, (b) Seebeck coefficients and (c) power factors.

The temperature dependence of the total thermal conductivity κ of $Co_{1-x}Cu_xSbS_4$ (x =0, 0.04 0.06) samples is presented in Fig. 5a. A relatively high thermal conductivity was observed for all samples over the entire temperature range measured. The un-substituted CoSbS posed a thermal conductivity of 3.96 W/mK at room temperature, and this value decreased to 3.44 W/mK for Cu-substituted $Co_{1-x}Cu_xSbS_4$ at x = 0.06. As shown in Fig. 5a, thermal conductivity decreased with temperature and reached a value around 2 W/mK for all samples at 723 K, which is lower than the previously reported values for CoSbS at this temperature [24-27]. The lower thermal conductivity can be mainly attributed to the lower density and higher level of porosity in our samples. Fig. 5b shows the temperature-dependent TE figure of merit *ZT* for

[DOI: 10.22068/ijmse.16.4.20]

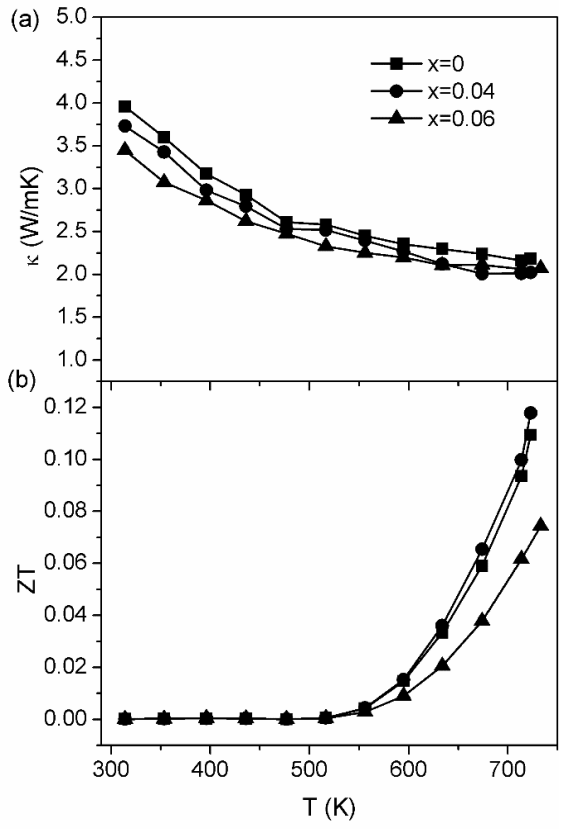

Fig. 5. Temperature dependence of (a) total thermal conductivities and (b) TE figure of merit ZT for $Co_{1-x}Cu_xSbS_4$ solid solutions.

$Co_{1-x}Cu_xSbS_4$ samples. A *ZT* value of 0.11 was obtained for un-doped CoSbS sample at 723 K. Cu substitution had a very minor effect on *ZT* values. A slightly higher *ZT* value of 0.12 was obtained for $Co_{0.06}Cu_{0.04}SbS_4$ solid solution at 723 K.

4. CONCLUSIONS

This study investigated the TE properties of $Co_{1-x}Cu_xSbS$ (x = 0, 0.04, 0.06) synthesized by a new route. Pure CoSbS was obtained after 2 h mechanical alloying of precursor powders followed by optimized annealing at 650 ºC for 1 h. All samples exhibited p-type conduction at room temperature and a reversible p- to n-type transition at 500 K. A regular decrease in the electrical resistivity and Seebeck coefficient was observed upon Cu substitution for Co. A maximum power factor of 0.3299 mW/mK^2 was obtained for un-doped CoSbS at 723 K. Thanks to the nanocrystalline nature and lower density of our samples, a thermal conductivity lower than those previously published were obtained for CoSbS. The maximum *ZT* value of 0.12 was obtained for $Co_{0.06}Cu_{0.04}SbS_4$ solid solution at 723 K.

REFERENCES

1. Li, Q., Zhang, L., Yin, J., Sheng, Z., Chu, X., Wang, F. and Zhu, F., "Study on the thermoelectric performance of polycrystal SnSe with Se vacancies". J. Alloys Compd., 2018, 745, 513-518.
2. Ahmed, R., Masuri, N. S., Haq, B. U., Shaari, A., AlFaifi, S., Butt, F. K., Muhamad, M. N., Ahmed, M. and Tahir, S. A., "Investigations of electronic and thermoelectric properties of half-Heusler alloys XMgN (X= Li, Na, K) by first-principles calculations". Mater. Des., 2017, 136, 196-203.
3. Hwang, J. Y., Ahn, J. Y., Lee, K. H. and Kim, S. W., "Structural optimization for thermoelectric properties in Cu-Bi-S pavonite compounds". J. Alloys Compd., 2017, 704, 282-288.
4. Ortega, S., Ibáñez, M., Liu, Y., Zhang, Y., Kovalenko, M. V., Cadavid, D. and Cabot, A., "Bottom-up engineering of thermoelectric nanomaterials and devices from solution-processed nanoparticle building blocks". Chem. Soc. Rev., 2017, 46, 3510-3528.
5. Zhang, K., Zhang, Q., Wang, L., Jiang, W. and Chen, L., "Enhanced thermoelectric performance of Se-doped PbTe bulk materials via nanostructuring and multi-scale hierarchical architecture". J. Alloys Compd., 2017, 725, 563-572.
6. Liu, Y., Zhang, Y., Ortega, S., Ibáñez, M., Lim, K. H., Grau-Carbonell, A., Martí-Sánchez, S., Ng, K. M., Arbiol, J., Kovalenko, M. V. and Cadavid, D., "Crystallographically textured nanomaterials produced from the liquid phase sintering of $Bi_xSb_{2-x}Te_3$ Nanocrystal Building Blocks". Nano Lett., 2018, *18*, 2557-2563.
7. Ju, H. and Kim, J., Preparation and structure dependent thermoelectric properties of nanostructured bulk bismuth telluride with graphene. J. Alloys Compd., 2016, 664, 639-647.
8. Fu, T., Yue, X., Wu, H., Fu, C., Zhu, T., Liu, X., Hu, L., Ying, P., He, J. and Zhao, X., "Enhanced thermoelectric performance of PbTe bulk materials with figure of merit *ZT*> 2 by multi-functional alloying". J. Materiomics, 2016, 2, 141-149.
9. Ibáñez, M., Luo, Z., Genç, A., Piveteau, L., Ortega, S., Cadavid, D., Dobrozhan, O., Liu, Y., Nachtegaal, M., Zebarjadi, M. and Arbiol, J.,

[DOI: 10.22068/ijmse.16.4.20]

"High-performance thermoelectric nanocomposites from nanocrystal building blocks". Nat. Commun., 2016, 7, 10766.
10. Mozharivskyj, Y., Pecharsky, A. O., Bud'ko, S. and Miller, G. J., "A promising thermoelectric material: Zn_4Sb_3 or $Zn_{6-\delta}Sb_5$. Its composition, structure, stability, and polymorphs. Structure and stability of $Zn_{1-\delta}Sb$. Chem". Mater., 2004, 16, 1580-1589.
11. Chetty, R., Bali, A. and Mallik, R. C., "Tetrahedrites as thermoelectric materials: an overview". J. Mater. Chem. C, 2015, 3, 12364-12378.
12. Qiu, P., Zhang, T., Qiu, Y., Shi, X. and Chen, L., "Sulfide bornite thermoelectric material: a natural mineral with ultralow thermal conductivity". Energy Environ. Sci., 2014, 7, 4000-4006.
13. Lu, X., Morelli, D. T., Xia, Y., Zhou, F., Ozolins, V., Chi, H., Zhou, X. and Uher, C., "High performance thermoelectricity in earth-abundant compounds based on natural mineral tetrahedrites". Adv. Energy Mater., 2013, 3, 342-348.
14. Barbier, T., Lemoine, P., Gascoin, S., Lebedev, O. I., Kaltzoglou, A., Vaqueiro, P., Powell, A. V., Smith, R. I. and Guilmeau, E., "Structural stability of the synthetic thermoelectric ternary and nickel-substituted tetrahedrite phases". J. Alloys Compd., 2015, 634, 253-262.
15. Coughlan, C., Ibanez, M., Dobrozhan, O., Singh, A., Cabot, A. and Ryan, K. M., "Compound copper chalcogenide nanocrystals". Chem. Rev., 2017, 117, 5865-6109.
16. Heo, J., Laurita, G., Muir, S., Subramanian, M. A. and Keszler, D. A., "Enhanced thermoelectric performance of synthetic tetrahedrites. Chem. Mater., 2014, 26, 2047-2051.
17. Lu, X., Morelli, D. T., Xia, Y. and Ozolins, V., "Increasing the thermoelectric figure of merit of tetrahedrites by Co-doping with nickel and zinc". Chem. Mater., 2015, 27, 408-413.
18. Lu, X. and Morelli, D., "The effect of Te substitution for Sb on thermoelectric properties of tetrahedrite". J. Electron. Mater., 2014, 43, 1983-1987.
19. Chetty, R., Bali, A., Naik, M. H., Rogl, G., Rogl, P., Jain, M., Suwas, S. and Mallik, R. C., "Thermoelectric properties of Co substituted synthetic tetrahedrite". Acta Mater., 2015, 100, 266-274.
20. Guélou, G., Powell, A. V. and Vaqueiro, P., "Ball milling as an effective route for the preparation of doped bornite: synthesis, stability and thermoelectric properties". J. Mater. Chem. C, 2015, 3, 10624-10629.
21. Zhang, A., Shen, X., Zhang, Z., Lu, X., Yao, W., Dai, J., Xie, D., Guo, L., Wang, G. and Zhou, X., "Large-scale colloidal synthesis of Cu_5FeS_4 compounds and their application in thermoelectrics". J. Mater. Chem. C, 2017, 5, 301-308.
22. Ostovari Moghaddam, A., Shokuhfar, A., Cabot, A. and Zolriasatein, A., "Synthesis of bornite Cu5FeS4 nanoparticles via high energy ball milling: Photocatalytic and thermoelectric properties". Powder Technol., 2018, 333, 160-166.
23. Ostovari Moghaddam, A., Shokuhfar, A. and Cabot, A., "Thermoelectric properties of nanostructured bornite $Cu_{5-x}Co_xFeS_4$ synthesized by high energy ball milling". J. Alloys Compd., 2018, 750, 1-7.
24. Ostovari Moghaddam, A., Shokuhfar, A., Guardia, P., Zhang, Y. and Cabot, A., "Substantial role of doping in the thermoelectric and hardness properties of nanostructured bornite, Cu_5FeS_4". J. Alloys Compd., 773, 2019, 1064-1074.
25. Long, S. O., Powell, A. V., Vaqueiro, P. and Hull, S., "High thermoelectric performance of bornite through control of the Cu (II) content and vacancy concentration". Chem. Mater., 2018, 30, 456-464.
26. Chmielowski, R., Bhattacharya, S., Xie, W., Pere, D., Jacob, S., Stern, R., Moriya, K., Weidenkaff, A., Madsen, G. K. H. and Dennler, G., "High thermoelectric performance of tellurium doped paracostibite". J. Mater. Chem. C, 2016, 4, 3094-3100.
27. Chmielowski, R., Bhattacharya, S., Jacob, S., Péré, D., Jacob, A., Moriya, K., Delatouche, B., Roussel, P., Madsen, G. and Dennler, G., "Strong reduction of thermal conductivity and enhanced thermoelectric properties in $CoSbS_{1-x}Se_x$ paracostibite". Sci. Rep., 2017, 7, 46630.
28. Liu, Z., Geng, H., Shuai, J., Wang, Z., Mao, J., Wang, D., Jie, Q., Cai, W., Sui, J. and Ren, Z., "The effect of nickel doping on electron and phonon transport in the n-type nanostructured thermoelectric material CoSbS". J. Mater. Chem. C, 2015, 3, 10442-10450.
29. Yao, W., Yang, D., Yan, Y., Peng, K., Zhan, H., Liu, A., Lu, X., Wang, G. and Zhou, X., "Synergistic Strategy to Enhance the Thermoelectric Properties of $CoSbS_{1-x}Se_x$ Compounds via Solid Solution". ACS Appl. Mater. Interfaces, 2017, 9, 10595-10601.

[DOI: 10.22068/ijmse.16.4.20]